Volume 1 | Number 1 | Jan 2013 | Pages 1–100

Dalton Transactions

An international journal of inorganic chemistry
www.rsc.org/dalton

ROYAL SOCIETY OF CHEMISTRY

ROYAL SOCIETY OF CHEMISTRY

www.rsc.org/dalton

Journal Name

ARTICLE

Hierarchical nanospheres based on Pd nanoparticles dispersed on carbon coated magnetite cores with a mesoporous ceria shell: a highly integrated multifunctional catalyst

Yinle Li, Zhuqing Zhang, Jianfeng Shen and Mingxin Ye*

The designing and fabrication of core-shell nanostructures with steerable morphologies and tailored performances have aroused abundant scientific research for organic transformations. We report here the preparation of multifunctional and highly efficient core-shell microspheres, which bear a carbon-protected magnetic Fe_3O_4 core, a transition layer of active Pd nanoparticles (NPs) and an outer shell of mesoporous CeO_2 ($mCeO_2$). The composition and structure of as-prepared $Fe_3O_4@C-Pd@mCeO_2$ were thoroughly characterized by X-ray photoelectron spectroscopy, Transmission electron microscopy, Scanning electron microscopy, X-ray diffraction, Fourier-transform infrared spectroscopy and Brunauer-Emmett-Teller measurement, respectively. The well-designed microspheres have high dispersibility, convenient magnetic separability and good reusability as heterogeneous nanoreactors due to their unique structure. We illustrate the high efficiency of this nanocomposites in mediating the Suzuki-Miyaura cross-coupling reaction and the reduction reaction of 4-nitrophenol (4-NP). The enhanced catalytic activity can be attributed to the synergistic effect between the CeO_2 nanoparticles and noble metal NPs. The mechanism was further proposed to explain the improved catalytic activity. This peculiar core-shell nanostructure renders the nanospheres to be an approachable and fancy catalyst system for various catalytic organic industry processes.

Introduction

Owing to the extraordinary advantages of unique optical, electrochemical and catalytic properties, noble metal NPs make themselves become the promising materials for underlying applications in various fields[1-5]. In particular, with the property of the high surface-to-volume ratio and the superiority of incorporating the differentia of homogeneous and heterogeneous catalysis[6], employing noble metal nanoparticles (such as Pd[7], Au[8], Pt[9], Ag[10]) in catalytic reaction have aroused enormous scientific research. However, naked noble metal NPs tend to aggregate and sinter, leading the loss of catalytic activity under reaction conditions. Therefore, solving this predicament and promoting environmental consciousness are imperative parts of chemical researches[11-14], and also enhancing efficiency of the catalysts in chemical reactions under a friendly condition with recycling using is equally important. Loading noble metal NPs on the special surface of supports is one of the best approaches to boost the efficiency and recyclability of the catalysts[15-16].

Currently, the introduction of magnetic NPs in various solid matrices permits the assembly of well-known programs for catalyst

heterogenization with magnetic separation[17-18]. Magnetite is an ideal support, easily prepare, having a proper active surface for the immobilization of metals and ligands, which can be isolated by magnetic decantation after the completion of a reaction, thus making it a better sustainable catalyst[19-21]. In the last few years, Magnetic core-shell nanostructure[22-23], a special type of universal functional composite with distinct microstructure, has shown a great application for loading noble metal NPs[24-29]. Generally, silica or carbon as a protecting shell is hired to coat the magnetic particles to make the shape of core-shell nanostructured ($Fe_3O_4@SiO_2$ or $Fe_3O_4@C$)[30-33]. Meanwhile, silica or carbon shell can prevent the magnetic particles from losing their magnetic properties in acidic environments and provide numerous functionalized groups for further modification. Several noble metal NPs dispersed on the surface of $Fe_3O_4@SiO_2$ or $Fe_3O_4@C$ core-shell nanostructure have been reported in an attempt to fulfill easy separation and recyclable catalytic processes including methanol oxidation[34], Fenton-like catalysis[35], hydrogenation[36] and cross-coupling reactions[31]. However, the active metal NPs on the surface of core-shell nanostructure directly expose in reaction condition can be easily leached. The novel mesoporous "shell-in-shell" hierarchical structures composed of mesoporous outermost shell and protected magnetic inside core-shell structure with the ultrafine active metal NPs distributed on the internal and external surface endows the nanocatalyst with high stability, reducing the leaching of active metal NPs, and independent cavity formed by two shells[36-37]. Zhao et

al[38] synthesized multicomponent and multifunctional Fe_3O_4@C-Pd@mSiO$_2$ hierarchical "shell-in-shell" structures for Suzuki-Miyaura coupling reaction. According to our investigation, there is only a little report about the assembling of magnetic core-shell nanocatalyst with active hierarchical structures, because the precise control of the morphology, structure and assembly process of each section is always very troublesome.

Herein, we report novel well-defined hierarchical "shell-in-shell" structures of Fe_3O_4@C-Pd@mCeO$_2$ consisting of a core of carbon-protected magnetite particles, a transition layer of confined catalytic Pd nanoparticles, and an outer shell of mesoporous CeO$_2$. The outermost CeO$_2$ shell can not only prevent active Pd NPs from aggregating, sintering and leaching, but also improve the catalytic activity due to a strong synergistic effect between the CeO$_2$ nanoparticles and noble metal NPs[39]. The well-designed Fe_3O_4@C-Pd@mCeO$_2$ hierarchical core-shell structures possess the advantages of large magnetization, highly open mesoporous and well dispersible in water. The multifunctional catalytic activities are systematically tested for catalyzing the Suzuki-Miyaura cross-coupling reaction and the reduction reaction of 4-NP. The studies reveal that the CeO$_2$ nanoparticles and noble metal NPs exhibit excellent synergetic catalytic performance and the good reusability of the system by the magnetic separation for both of the reactions. Our results therefore afford a general way based on a hierarchical core-shell structure for the preparation of high performance magnetic catalysts loaded with noble metal NPs, which will be a very useful tool for various catalytic organic industry processes.

Experimental

Materials

Ferric chloride hexahydrate (FeCl$_3$·6H$_2$O), Trisodium citrate, Palladium(II) chloride (PdCl$_2$), Sodium acetate (NaAc), Ethylene glycol (EG), glucose, Cerium(III) nitrate hexahydrate (Ce(NO$_3$)$_3$·6H$_2$O), Hexamethylene tetramine (HMT), 4-nitrophenol (4-NP), Arylboronic acid, Aryl halide were bought from Sinopharm Chemical Reagent (Shanghai, China). All of the reagents were of analytical grade and directly used without further purification.

Synthesis of core-shell Fe_3O_4@C nanoparticles

The magnetic Fe_3O_4 nanoparticles modified by trisodium citrate were prepared according to the work reported by Zhao[38]. Fe_3O_4@C nanoparticles were synthesized by a versatile hydrothermal method. Briefly, 1 g of as-prepared Fe_3O_4 nanoparticles and 3.24 g of glucose were dispersed into 60 mL water. After ultrasonication for 30 min, the mixture was transferred to a Teflon-lined stainless-steel autoclave (90 mL volume), and then sealed to heat at 180 ^{o}C for 4 h. The products were collected from the solution through an external magnet and washed with deionized water three times, ethanol three times, and then vacuum dried at 60 ^{o}C for overnight.

Synthesis of core-shell Fe_3O_4@C-Pd nanoparticles

Fe_3O_4@C-Pd nanoparticles were synthesized by the deposition-precipitation method. Typically, 100 mg Fe_3O_4@C nanoparticles were dispersed in 120 mL 1:1 water/ethanol with ultrasound for 30 min. Then, 5 mL 0.01 M PdCl$_2$ ethanol dispersion was added into the above solution. After ultrasound for another 30 min, Than the obtained mixture was then mechanical stirred in 100 ^{o}C for 50 min,

and then allowed to cool to room temperature. The products were separated by applying an external magnet and washed with deionized water three times, ethanol three times, and then vacuum dried at 60 ^{o}C for overnight.

Synthesis of core-shell Fe_3O_4@C-Pd @mCeO$_2$ nanoparticles

100 mg Fe_3O_4@C-Pd nanoparticles were dispersed and sonicated for 30 min in 60 mL ethanol. 200 mg Ce(NO$_3$)$_3$·6H$_2$O was dissolved in 60 mL ethanol, then mixed together under an ultrasound treatment process for 10 min. Subsequently, 0.8 g HMT dissolved in 80 mL pure water was added to the mixture solution with ultrasound for another 15 min. The mixture was then mechanical stirred for 2 h at 70 ^{o}C. The resultant products were separated with a magnet, and washed with water 5 times to remove any potential ionic remnants. Finally, the products vacuum dried at 60 ^{o}C for overnight. The power was calcined at 400 ^{o}C for 2 h to obtain Fe_3O_4@C-Pd@mCeO$_2$ nanoparticles. The product was decomposed in concentrated nitric acid, and then analysed via inductively couple plasma atomic emission spectrometer (ICP-AES) to determine the content of Pd (3.05 wt%).

The synthesis process of Fe_3O_4@C@mCeO$_2$ nanoparticles are the same to Fe_3O_4@C-Pd@mCeO$_2$ nanoparticles without Pd nanoparticles.

Suzuki-Miyaura cross-coupling reactions

The Fe_3O_4@C-Pd@mCeO$_2$ catalyst (10 mg), aryl halide (1.0 mmol), arylboronic acid (1.2 mmol) and potassium carbonate (2 mmol) added to Schlenk tube containing a magnetic stirrer (in the case of stirring, the catalyst has good solubility in our choice solvent), solvent (5 mL) was then added. The mixture was stirred at 80 ^{o}C in air. The reaction process was monitored by GC at a fixed time interval. The catalyst was separated from the mixture with a magnet, washed several times with water and ethanol, and then dried in vacuum at 60 ^{o}C for overnight. The recycling experiment was tested following the same procedures.

Reduction of 4-NP

The reduction of 4-NP was tested in a quartz cuvette and monitored by a UV-vis spectroscopy (Shimadzu UV-3600) at room temperature. In a typical procedure, 4.0 mg of Fe_3O_4@C-Pd@mCeO$_2$ composites was homogeneously dispersed into the 4.0 mL 4-NP solution (10 mg L^{-1}), followed by a quick injection of 1 mL of fresh NaBH$_4$ solution (10 mg mL^{-1}) under stirring. The color of the mixture solution gradually changed from yellow to colorless, indicating that the Fe_3O_4@C-Pd@mCeO$_2$ composites catalyzed the reduction of 4-NP. After stirring every ten seconds, the mixture was rapidly moved to quartz cell to monitor the reduction progress by recording the UV-vis absorption spectra of the solution. Since the 4-NP has a strong absorption peak at 400 nm in the presence of NaBH$_4$, the product of 4-aminophenol has a moderate absorption peak at 295 nm.

In the recycling study, the Fe_3O_4@C-Pd@mCeO$_2$ composites were separated from the mixture by using a magnet after the reduction reaction completely finished. When washing with ethanol 3 times and water 3 times, they were utilized in the next reaction run similar to the above reduction process.

Characterization

FT-IR was recorded over the wavenumber ranging from 4000 to 400

cm^{-1} on a Nicolet IS10 spectrometer, and solid samples were measured with KBr disks. XRD analyses were recorded on D/max-γB diffractometer using Cu Kα radiation. Transmission electron microscopy (TEM) measurements were taken on a TEOL2010F microscope handled at 200 kV. The samples were dispersed in ethanol and transferred onto holey carbon films supported with a Cu grid for TEM measurements. High resolution transmission electron microscopy (HR-TEM) and scanning transmission electron microscopy (STEM) images were tested on a JEM-2100F scanning transmission electron microscope to characterize the morphologies of the particles. Scanning electron microscopy (SEM) images were obtained from Philips XL30FEG. The samples were dispersed in ethanol and transferred onto silicon chip for SEM measurements. N$_2$ sorption isotherms were measured with a Micromerits Tristar 3000 analyzer at 77 k. The powder was degassed at 200 ºC in a vacuum for 10 h. By using the Barrett–Joyner–Halenda (BJH) model, the pore volumes and the pore size distributions were acquired from the adsorption branches of the isotherms. The Brunauer-Emmett-Teller (BET) method was used to count the specific surface areas using adsorption date. The magnetization curve of the sample was recorded on a superconducting quantum interference device (SQUID) magnetometer (Quantum Design MPMS XL-7) at 300 K. X-ray photoelectron spectroscopy (XPS) was collected on XR 5 VG (UK) using a monochromatic Mg X-ray source. Binding energy standardization was based on C 1s at 284.6 eV.

Results and discussion
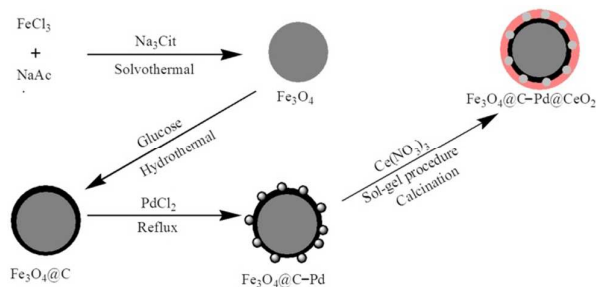
Scheme 1 Schematic of the preparation of Fe$_3$O$_4$@C-Pd@mCeO$_2$ composites

The procedure for the preparation of hierarchical core-shell nanospheres, designated as Fe$_3$O$_4$@C-Pd@mCeO$_2$, is shown in Scheme 1. First, the Fe$_3$O$_4$ nanoparticles modified by trisodium citrate were prepared via a rough solvothermal reaction grounded on a high temperature reduction of FeCl$_3$·6H$_2$O in the presence of EG and NaAc[38]. Then, a uniform carbon coating was fabricated on the surface of Fe$_3$O$_4$ nanoparticles through hydrothermal treatment with glucose as carbon source, resulting in core-shell Fe$_3$O$_4$@C nanospheres. After that, Pd NPs were recommended on the surface of the carbon-protected Fe$_3$O$_4$ nanospheres by refluxing in an ethanol/water solution using PdCl$_2$ as the precursor without any additional reducing agents[22]. The prepared Pd-immobilized Fe$_3$O$_4$@C nanospheres were denoted as Fe$_3$O$_4$@C-Pd. Finally, Ce(NO$_3$)$_3$·6H$_2$O was used as a cerium source and HMT was applied to slowly produce OH$^-$ so as to get a homogenous CeO$_2$ coating surrounding the Fe$_3$O$_4$@C-Pd nanospheres through an assembly sol-gel process. Subsequently, HMT was removed by a calcinations

process and a porous CeO$_2$ shell can be obtained[40], resulting in Fe$_3$O$_4$@C-Pd@mCeO$_2$ nanospheres with a sandwich-like structure.
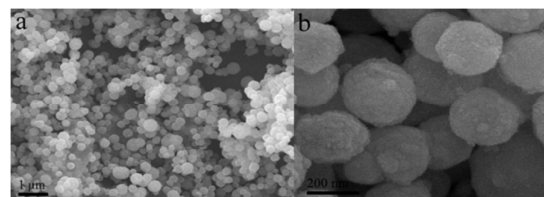
Fig. 1 SEM image of Fe$_3$O$_4$@C-Pd@mCeO$_2$ (a) 1 μm; (b) 200 nm
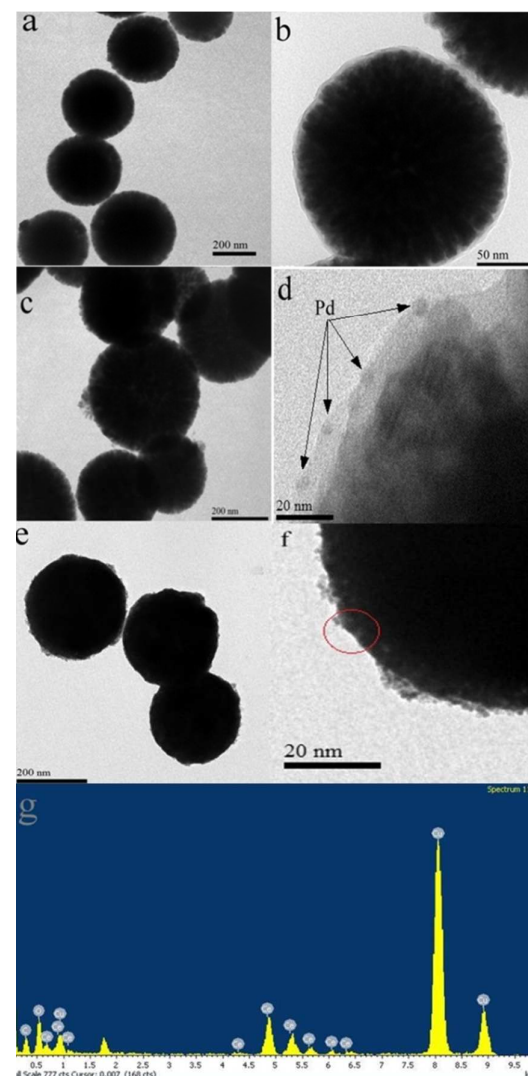
Fig. 2 TEM image of (a, b) Fe$_3$O$_4$@C nanospheres; (c, d) Fe$_3$O$_4$@C-Pd nanospheres; (e, f) Fe$_3$O$_4$@C-Pd@mCeO$_2$ nanospheres; (g) EDX corresponding to the red circular region of panels f

The morphology and structure of the as-prepared composites were investigated by SEM and TEM. Fig. 1a and 1b shows the SEM images of the Fe$_3$O$_4$@C-Pd@mCeO$_2$ nanospheres. It can be seen from the images that the Fe$_3$O$_4$@C-Pd@mCeO$_2$ nanospheres has the sizes in the range of 250-300 nm and a spherical shape. Fig. S1 show the EDX spectrum of Fe$_3$O$_4$@C-Pd@mCeO$_2$ nanospheres. The

loading amount of Pd in the $Fe_3O_4@C-Pd@mCeO_2$ catalyst is estimated to be 0.35 atom% from EDX analysis. Fig. 2a and 2b shows the TEM images of the $Fe_3O_4@C$ after the hydrothermal reaction of Fe_3O_4 NPs, a thin carbon layer of ~8 nm thickness was formed on Fe_3O_4 nanospheres, resulting in core-shell $Fe_3O_4@C$ nanospheres. After the deposition of Pd NPs, numerous monodispersed Pd NPs were uniformly deposited on the carbon shell with an average size of 4~5 nm, producing $Fe_3O_4@C-Pd$ nanospheres (Fig. 2c and 2d). After further deposition of a homogenous CeO_2 shell, $Fe_3O_4@C-Pd@mCeO_2$ nanospheres with regular spherical morphology are obtained (Fig. 2e and 2f).

However, as the high electron density of polycrystalline CeO_2[41], the small size of Pd NPs and the specific core-shell architecture, it is difficult to recognize the interface between Pd NPs and CeO_2. Therefore, the encapsulated Pd NPs cannot be visualized evidently from the TEM image of $Fe_3O_4@C-Pd@mCeO_2$ nanospheres[41]. Additionally, the selected areas of the red circular region of panels Fig. 2g provides EDX results shows that the main existed element in the outmost shell of the nanospheres is cerium. Therefore, The HR-TEM images shown in Fig. 3a and 3b further demonstrate that the relatively crude surface is composed of ultrafine Pd and CeO_2 nanocrystallites with main sizes of approximately 4.5 nm and 5 nm. The lattice fringes are obviously visible with d-spacings of about 0.32 nm and 0.21 nm, which readily indexes to the lattice spacings of the (111) planes of the cubic uorite phase of CeO_2 and the (111) lattice planes of Pd NPs[42]. Additionally, scanning transmission electron microscopy (STEM) and EDS elemental mapping are also implemented to uncover the elemental distribution in these structured microspheres. The STEM images in Fig. 3c reveal that the structure is core-shell structured microspheres. The corresponding EDS mapping images results indicate that the elements Fe, Ce, O and Pd are dispersed evenly throughout the whole spheres. The elements Pd and Ce are thoroughly distributed in the outermost surface of the microspheres, which confirms the hierarchical core-shell structure of $Fe_3O_4@C-Pd@mCeO_2$ as obtained by the elaborate assembly procedures illustrated in Scheme 1.
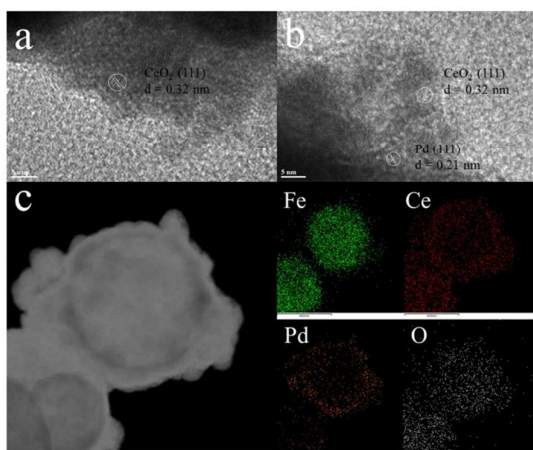

Fig. 3 (a, b) HR-TEM images of $Fe_3O_4@C-Pd@mCeO_2$ nanospheres, (c) HADDF-STEM images of $Fe_3O_4@C-Pd@mCeO_2$ nanospheres and corresponding EDS mapping images.

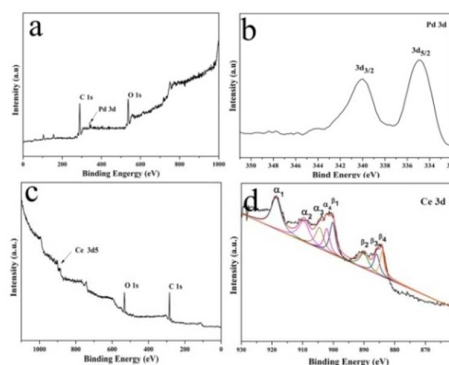**Fig. 4** XPS spectra of (a) $Fe_3O_4@C-Pd$ nanospheres and (b) Pd 3d; (c) $Fe_3O_4@C-Pd@mCeO_2$ nanospheres and (d) Ce 3d
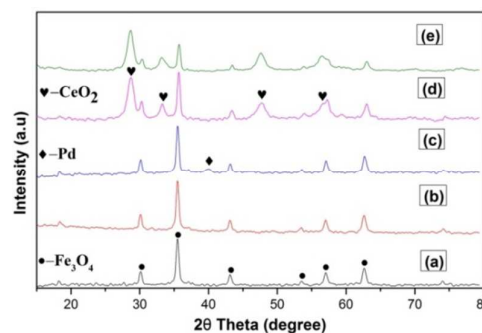
Fig. 5 XRD pattern of (a) Fe_3O_4 nanospheres, (b) $Fe_3O_4@C$ nanospheres, (c) $Fe_3O_4@C-Pd$ nanospheres, (d) $Fe_3O_4@C@mCeO_2$ nanospheres, (e) $Fe_3O_4@C-Pd@mCeO_2$ nanospheres
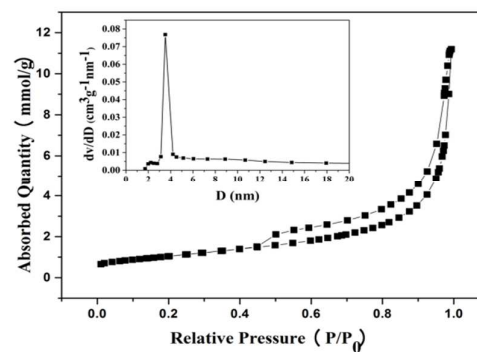
Fig. 6 Nitrogen adsorption-desorption isotherm plots of $Fe_3O_4@C-Pd@mCeO_2$ and pore size distribution curves of $Fe_3O_4@C-Pd@mCeO_2$ (inset in the Fig. 6)

To further confirm the presence of Pd NPs and CeO_2 shell, surface analysis of the prepared nanospheres was measured using XPS (Fig. 4). In Fig. 4a, it was hard to observe the peak of iron element from the XPS spectrum of $Fe_3O_4@C-Pd$ nanospheres, suggesting that the Fe_3O_4 nanospheres were thoroughly coated by a carbon layer to form core-shell structure[42]. The regional XPS spectrum of Fig. 4b showed two peaks at 341.1 and 335.7 eV, which were corresponded to Pd(0) of $3d_{3/2}$ and $3d_{5/2}$, respectively. This indicated that the Pd(0) NPs were formed on the surface of $Fe_3O_4@C$ nanospheres[42]. The XPS spectrum of $Fe_3O_4@C-Pd@mCeO_2$ nanospheres (Fig. 4c) reveals

that carbon, oxygen and cerium are present in the surface of the nanospheres. Concerning the characteristic signals of the Ce3d spectrum, the four primary $3d_{3/2}$ peaks located at around 917.8 eV, 907.8 eV, 904.5 eV and 901.6 eV matching the α_1, α_2, α_3 and α_4 components, while the $Ce3d_{5/2}$ peaks located at around 898.7 eV, 888.0 eV, 885.3 eV, and 883.0 eV in accordance with β_1, β_2, β_3 and β_4, respectively (Fig.4d)[43]. Both the signals α_3 and β_3 are the characteristic peaks of Ce^{3+}, while the other peaks are corresponding with the characteristic peaks of Ce^{4+}. The presence of Ce^{3+} can be conducive to the synergistic effect between the CeO_2 nanoparticles and noble metal NPs[44]. The Ce^{3+} : Ce^{4+} ratio in the Fe_3O_4@C-Pd@mCeO$_2$ catalyst was ca. 18%.

Fig. S2 shows the FT-IR spectra of Fe_3O_4 nanospheres, core-shell Fe_3O_4@C nanospheres, Fe_3O_4@C-Pd nanospheres and Fe_3O_4@C-Pd@mCeO$_2$ nanospheres synthesized in this work. The FT-IR spectrum of magnetite nanoparticles (Fig. S2a) shows absorption bands at 583 and 1650 cm^{-1}, which are attributed to the vibration mode of Fe-O and the carbonyl group of trisodium citrate[45]. The bands around 3400 cm^{-1} are ascribed to the OH vibrating. From Fig. S1b, for core-shell Fe_3O_4@C nanoparticles, the peaks around 1620 cm^{-1} are related to the aromatization of glucose during hydrothermal treatment[46]. From Fig. S2c and S2d, the absorption peaks of Fe_3O_4@C-Pd nanospheres and Fe_3O_4@C-Pd@mCeO$_2$ nanospheres are similar to the Fe_3O_4@C nanospheres. However, it is noteworthy that the intensity of absorption peaks was significantly weaker than that of Fe_3O_4@C nanoparticles after anchored with Pd nanoparticles and coated by CeO_2.

The phase and composition of the resulting products are profoundly characterized by XRD in Fig. 5. In Fig. 5a, all the peaks at about 29.9°, 35.3°, 43.0°, 56.9°and 62.5°are associated with Fe_3O_4 (220), (311), (440), (511) and (220) peaks of face centered cubic. From the Fig. 5b, there is no obvious change in XRD of Fe_3O_4@C nanospheres compare with Fe_3O_4 nanospheres. On the XRD patterns of Fe_3O_4@C-Pd in Fig. 5c, in addition to the peaks of Fe_3O_4 core, additional peaks located near 40.0° are well-indexed to face centered Pd (111) peaks (JCPDS No. 05-0681)[42]. Fig. 5d and 5e show the XRD patterns of Fe_3O_4@C@mCeO$_2$ nanoparticles and core-shell Fe_3O_4@C-Pd@mCeO$_2$ nanoparticles, both of the figures indicate the peaks at 28.7°, 33.2°, 47.8°, 56.3°, are corresponding to the (111), (200), (220), (311), Bragg diffraction of CeO_2 (JCPDS No.34-0394)[39]. There are no diffraction peaks matching to Pd nanoparticles in the Fig. 5e owing to their high dispersity and the low content loading[42].

The magnetic performances of the samples are investigated using a SQUID magnetometer at 300 K from -20000 to 20000 Oe. Fig. S3 shows the magnetization curves of Fe_3O_4 nanospheres (black), Fe_3O_4@C nanospheres (red), Fe_3O_4@C-Pd nanospheres (blue) and Fe_3O_4@C-Pd@mCeO$_2$ nanoparticles (pink), respectively. At 300 K, the saturation magnetization value is 74.9, 25.5, 24.6 and 21.3 emu per g, respectively. The inset in Fig. S3 shows the photograph of the dispersion of 5 mg/mL Fe_3O_4@C-Pd@mCeO$_2$ nanospheres in water before and after magnetic separation. To further analysis of the pore size distribution, BET measurement was carried out. As shown in Fig. 6, the N_2 adsorption–desorption isotherms of the Fe_3O_4@C-Pd@mCeO$_2$ composites exhibit representative type-IV curves, and the BET surface area is about 85 m^2 g^{-1}. The pore size distribution shows the pores size mostly range from 2.0 to 4.5 nm with an intense

peak appearing at around 3.5 nm, indicating a mesoporous CeO_2 shell. This result is in good agreement with the literature[40].

The successful synthesis of Fe_3O_4@C-Pd@mCeO$_2$ nanospheres can be attributed to the following outlines. Firstly, the Fe_3O_4 nanoparticles synthesized by solvothermal reaction are modified by citrate groups. Therefore, it can be highly dispersible in water and ethanol, favouring the further coating with other oxides or polymers[45]. Thus, a thin carbon layer can be readily coated on the Fe_3O_4 nanoparticles by the partial carbonization and polymerization of glucose under hydrothermal treatment[46]. Secondly, the existence of reductive groups (such as –OH and –CHO) in the carbon shell, rooted in the dehydration of the glucose can do duty for in-situ reduction of $PdCl_2$. Therefore, without additional reducing or linker agents are needed[22]. Thirdly, since the obtained Fe_3O_4@C–Pd nanospheres are hydrophilic and have a well dispersibility in ethanol and water, the subsequent surface coating of mesoporous CeO_2 can be achieved.

Based on the highly dispersible, we evaluate the efficiency of the catalytic by the Suzuki-Miyaura reaction (cross-coupling of 4-iodoanisole and phenylboronic acid) in a green medium of water or ethanol without any external promoters, phosphine ligands or biphasic media. From the results in table S1, we can see that a low-grade yield of the desired resultant was obtained by the Fe_3O_4@C@mCeO$_2$ without Pd NPs in an ethanol solvent (Table S1, entry 1). No obvious increase in yield was observed by increasing the reaction time (Table S1, entry 2). It is suggests that ceria has catalytic effect for Suzuki-Miyaura reaction[47]. In the solvent of water, the reaction did not occur at all (Table S1, entry 3). Significantly, the model reaction using Fe_3O_4@C–Pd or Fe_3O_4@C–Pd@mCeO$_2$ as the catalyst in water or ethanol or their mixture at 80 °C affording the desired product within 3 h in excellent isolated yield (Table S1, entry 4-9). Interestedly, other solvent, such as isopropanol, tetrahydrofuran, N,N-dimethylformamide, 1,4-dioxane, dimethyl sulfoxide, dimethylacetamide, toluene and dimethylbenzene, have fairly good catalytic effect for the same reaction with the Fe_3O_4@C–Pd@mCeO$_2$ as the catalyst (Table S2, entry 1-8).

To explore the expansion of this reaction, a series of aryl iodides were selected to react with phenylboronic acid under mixture solvent ethanol/water (1:1) and K_2CO_3. It is worth noting that Fe_3O_4@C-Pd@mCeO$_2$ as the catalyst can tolerate to a wider range of functional groups (Table 1, entry 2-7), such as –Me, –OCH$_2$CH$_3$, –OCF$_3$, –OH, –NH$_2$ and –COCH$_3$. Interestingly, aryl bromides delivered the products with high yields under identical conditions (Table 1, entry 8-9). However, aryl chloride is relatively rough for the same process with a medium yield (Table 1, entry 10-11). An array of substituted arylboronic acid substrates also underwent the cross-coupling reaction with aryl halide under our catalytic system (Table 1, entry 13-30). *Ortho*-methyl phenylboronic acid give good yields of 2-arylation product (Table 1, entry 13, 18, 23, 27) not hesitate to the steric hindrance. A satisfactory yield was also obtained by 1-naphthylboronic acid for the formation of 1-arylation naphthalane (Table 1, entry 16, 21, 26, 30). Both electron-withdrawing substituent (4-F) and electron-donating group (4-OCH$_3$) do not show inhibition effect under the same conditions (Table 1, entry 15, 17, 20, 25, 28, and 29).

We further compared the catalytic results gained in this

hierarchical "shell in shell" structure with other traditional supported Pd-based catalysts. Such as mesoporous carbon, polymer, silica or oxide. With the reaction of iodobenzene and phenylboronic acid as an example, the results were ticked off in Table S4. It can be obviously seen that the results achieved in this work are superior to others. Even though some of them also can acquire high yield, toxic solvents (such as DMF, CH_2Cl_2, or THF) or a long time were used. These solvent are less favorable to the mixture ethanol-water used in this work. The comparison of the catalytic performance between the catalyst of $Fe_3O_4@C$-Pd@mSiO$_2$[22] and our $Fe_3O_4@C$-Pd@mCeO$_2$ system has aslo been summarized in the Table S5. It can obviously observe that the catalytic performance of our $Fe_3O_4@C$-Pd@mCeO$_2$ system is better than the catalyst of $Fe_3O_4@C$-Pd@mSiO$_2$.
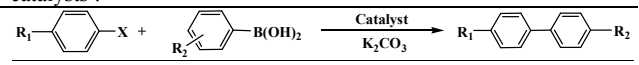
The catalytic property of $Fe_3O_4@C$-Pd@mCeO$_2$ composites was also evaluated by the reduction of 4-NP to 4-aminophenol (4-AP) in the presence of NaBH$_4$, which is one of the representative model reactions for estimating the catalytic activity of noble metal NPs[42]. As shown in Fig. 7a, when a trace amount of the $Fe_3O_4@C$-Pd@mCeO$_2$ nanocatalyst (2 mg) is introduced into the solution, the absorption peak at 400 nm decreases in a certain period of time and, simultaneously, a new absorption peak at 295 nm arises which can be attributed to the reduction of 4-NP and the emergence of 4-AP, respectively. For comparison, the catalytic activities of $Fe_3O_4@C$@mCeO$_2$ and $Fe_3O_4@C$-Pd as reference catalysts have also been investigated following the identical experimental conditions. The conversion can be directly read out from the curves made of the percentage of the absorbance intensity of 4-NP at an interval time to its initial absorbance intensity value, as displayed in Fig. 7b. It is obvious that $Fe_3O_4@C$@mCeO$_2$ exhibits negligible catalytic reduction activity, suggesting that the reduction reaction is mainly catalyzed by the Pd NPs; whereas the supported $Fe_3O_4@C$-Pd possesses inferior catalytic performance as compared to $Fe_3O_4@C$-Pd@mCeO$_2$ nanocomposites.

In addition to the outstanding catalytic activity, isolation and reusability of the catalyst, a considerable requirement for any practical application in accordance with spend and environmental protection[48-50], are the greatest merits in our study. In our systems, the catalysts can be lightly retrieved using an external magnet as is proved in Figure S3 inset. In order to investigate the reusability of the catalyst, both of the Suzuki-Miyaura reaction (cross-coupling of 4-iodoanisole and phenylboronic acid) and the reduction of 4-NP were chosen to be test. As illustrated in Fig S4a and S4b, the catalyst $Fe_3O_4@C$-Pd@mCeO$_2$ can be reused for ten times without obvious decrease of conversion and selectivity for both of the reactions by a simple magnetic separation. However, the results of Fig S4c andS4d reveal that the catalytic activity of the $Fe_3O_4@C$-Pd was found distinctly decrease during the recycling test after the two reduction process were repeated four times. Fig. S5 show the TEM images of $Fe_3O_4@C$-Pd@mCeO$_2$ after 10 runs of recycling experiments for the Suzuki reactions. The images indicate that the catalyst still keeps a spherical shape after recycling experiments.

Based on the above data, it could be readily concluded that the catalytic activity of $Fe_3O_4@C$-Pd@mCeO$_2$ is better than $Fe_3O_4@C$-Pd for the two reactions, it can be easily deduced that the $Fe_3O_4@C$-Pd@mCeO$_2$ core-shell nanostructure can effectively block the aggregation of the Pd NPs due to the robust protection of CeO$_2$ shells, thereby holding the high catalytic property of the Pd NPs. The

other more remarkable advantage of $Fe_3O_4@C$-Pd@mCeO$_2$ as a sharp compared to $Fe_3O_4@C$-Pd for mediating these reactions in solution is that the CeO$_2$ shells can effectively hinder the leaching of Pd NPs. The leaching test of Pd are analysed by ICP-AES after ten cycles, the results are listed in Table S3. Both reactions show determinable Pd loss, the trace content of Pd loss indicates that $Fe_3O_4@C$-Pd@mCeO$_2$ can be a reusable catalyst with additional anti-deactivation performance. This prominent characteristic can be confirmed by the very steady recycling catalytic activity test on $Fe_3O_4@C$-Pd@mCeO$_2$ (Fig. S4a and S4b) and its steady nanostructure.

Table 1 Suzuki reactions catalyzed by $Fe_3O_4@C$-Pd@mCeO$_2$ catalysts[a].

$$R_1 \text{—} X + R_2 \text{—} B(OH)_2 \xrightarrow[K_2CO_3]{Catalyst} R_1 \text{——} R_2$$

Entry	R$_1$	X	R$_2$	Yield[b]	TOF[d]
1	H	I	H	>99[c]	345.4
2	OCF$_3$	I	H	93	108.2
3	OH	I	H	95	116.3
4	OCH$_2$CH$_3$	I	H	92	107.0
5	NH$_2$	I	H	95	116.3
6	CH$_3$	I	H	95	116.3
7	COCH3	I	H	90	104.6
8	H	Br	H	95	116.3
9	CH$_3$	Br	H	90	104.6
10	H	Cl	H	50	58.2
11	CH$_3$	Cl	H	58	67.5
12	OCH$_3$	I	H	99	115.1
13	OCH$_3$	I	2-CH$_3$	90	104.6
14	OCH$_3$	I	4-CH$_3$	95	116.3
15	OCH$_3$	I	4-F	98	113.9
16	OCH$_3$	I	1-Naphthyl	85	98.9
17	COCH$_3$	I	4-OCH$_3$	82	95.4
18	COCH$_3$	I	2-CH$_3$	75	88.4
19	COCH$_3$	I	4-CH$_3$	88	102.3
20	COCH$_3$	I	4-F	93	108.2
21	COCH$_3$	I	1-Naphthyl	73	84.9
22	H	Br	4-OCH$_3$	88	102.3
23	H	Br	2-CH$_3$	68	79.1
24	H	Br	4-CH$_3$	78	90.7
25	H	Br	4-F	85	98.9
26	H	Br	1-Naphthyl	72	83.7
27	CH$_3$	Br	2-CH$_3$	75	88.4
28	CH$_3$	Br	4-OCH$_3$	85	98.9
29	CH$_3$	Br	4-F	86	100.0
30	CH$_3$	Br	1-Naphthyl	77	90.7

[a]Reaction conditions: aryl halide (1.0 mmol), arylboronic acid (1.2 mmol), potassium carbonate (2 mmol), 5 mL ethanol-water (1:1), 10 mg $Fe_3O_4@C$-Pd@mCeO$_2$ (Pd 3.05 wt%), at 80 °C for 3 h. [b] isolated yields. [c] 60 °C for 45 min. [d] TOF was defined as mol product mol^{-1} Pd h^{-1}.
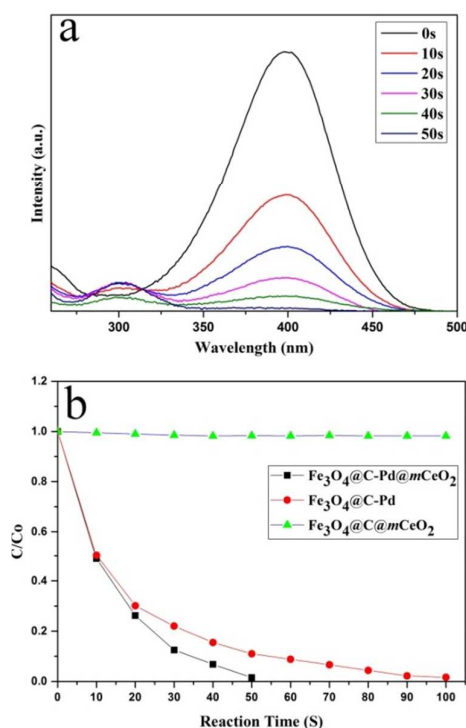
Fig. 7 (a) UV-vis spectra of the 4-NP and NaBH$_4$ solution in the presence of 2 mg Fe$_3$O$_4$@C-Pd@mCeO$_2$; (b) Performances of Fe$_3$O$_4$@C-Pd@mCeO$_2$, Fe$_3$O$_4$@C-Pd, Fe$_3$O$_4$@C@mCeO$_2$ nanocomposites for the reduction of 4-NP.

Over the past few decades, the comprehending of the interfacial effect between the noble metal NPs and the metal oxide supports is still ambiguous for heterogeneous reactions since multiple factors influence the catalytic activity of Pd nanocatalysts[51-52]. Many metal oxides have been employed as catalyst supports for the loading of the noble metal NPs to boost their catalytic activity and stability. CeO$_2$, which has a Ce^{4+}/Ce^{3+} redox cycle, is an ideal carrier due to its high oxygen storage capability, high oxygen mobility and low cost[53-54]. CeO$_2$ belong to the fluorite structure, in which each O^{2-} anion is encircled by a tetrahedron of Ce^{4+} cations situated at the center of a cubic array of equivalent O^{2-} atoms[55]. However, the non-stoichiometric oxides CeO$_{2-x}$, which gained through the wet-chemical synthesis, have a high density of oxygen vacancies. The partial elimination of O atoms from O^{2-} in the CeO$_2$ structure can form O-vacancy. The surplus electrons may either thoroughly delocalize in the conductor band, or distribute among a little Ce^{3+} cations to surround the O-vacancy, or located on the Ce^{4+} to form tervalence Ce[56]. Ce^{3+} is the rich electrons species and trends to afford electrons to metal catalysts[57]. Simultaneously, water dissociation occurs on the O-vacancy can produce the reactive OH groups[58]. Both Ce^{3+} species and OH groups are reactive δ^- sites, which can endow electrons to Pd NPs. Therefore, the Ce^{3+} fraction and O-vacancy concentration can be used to comprehend the synergistically catalytic effect for enhancing the catalytic activity.

A proposed reaction mechanism for the synergistically catalytic effect is illustrated in Schematic 1. During the wet-chemical synthesis process of the CeO$_2$, the Ce^{3+} cations species (which was also confirmed by XPS in Fig. 3d) and O-vacancy are formed. The active OH groups will be produced through the dissociation of water

on the O-vacancy sites[59]. Afterwards, the electron pair donors of the Ce^{3+} cations species and OH groups can be transferred to the Pd NPs via the electron-donating effect, leading to a higher electron density Pd NPs. So that to improve the first step of the oxidative addition reaction to form radical ligand Ar-Pd^{II}-Br. This step is regarded as the key step in the C–C coupling reactions[52]. The high density of electron of Pd NPs also can rapid catalyze the reduction of 4-NP.
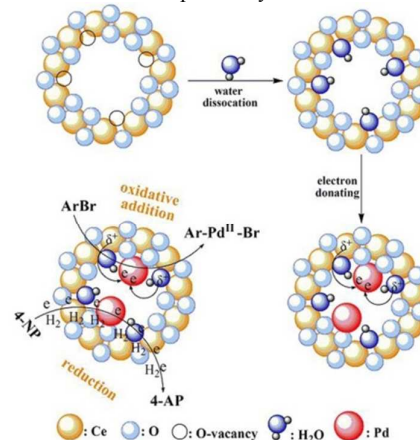
Schematic 1 the proposed mechanism for the synergistic effect between the CeO$_2$ NPs and Pd NPs with improved catalytic activity

Conclusions

In summary, we demonstrate a successful preparation of multicomponent and multifunctional Fe$_3$O$_4$@C-Pd@CeO$_2$ nanospheres with well-defined magnetic core-shell nanostructures, confined catalytic Pd NPs and accessible mesoporous CeO$_2$ by combining the hydrothermal method, interfacial in situ deposition and sol-gel process. The well-designed hierarchical nanospheres have high magnetization (21.3 emu/g), highly open mesoporous ($\sim$3.5 nm in diameter), smoothly restricted but uncovered catalytic Pd NPs that uniformly dispersed between the carbon-protected Fe$_3$O$_4$ core and mesoporous CeO$_2$ shell. The obtained multifunctional Fe$_3$O$_4$@C-Pd@CeO$_2$ nanospheres show excellent catalytic performance in the Suzuki-Miyaura cross-coupling reaction and the reduction of 4-nitrophenol both with convenient separability and remarkable reusability without loss activity after repeat ten times. Therefore, as a novel Pd-based catalyst system, this multifunctional core-shell nanostructure holds great promise for various catalytic reactions. Additionally, the design idea for the hierarchical nanomaterials can be expanded to the synthesis of other multicomponent nanomaterials with integrated and enhanced capabilities for various applications.

References

1   G. V. Hartland, *Chem. Rev.*, 2011, **111**, 3858–3887.
2   S N. Tian, Z. Zhou, S. Sun, Y. Ding and Z. L. Wang, *Science,* 2007, **316**, 732-735.
3   T. K. Sau, A. L. Rogach, F. Jäckel, T. A. Klar and J. Feldmann, *Adv. Mater.,* 2010, **22**, 1805-1825.
4   S. Linic, P. Christopher and D. B. Ingram, *Nat. Mater.*, 2011, **10**, 911-921.
5   A. Scholl, and A. Dionne. *Nature,* 2012, **483**. 421-427.

6   L. Chen, G. Chen, C. Leung, S. Yiu, C. Ko, E. Anxolabéhère-Mallart, M. Robert and T. Lau, *ACS Catal.,* 2015, **5**, 356-364.

7   L. Zhong, A. Chokkalingam, W. S. Cha, K. S. Lakhi, X. Su, G. Lawrence and A. Vinu, *Catal. Today,* 2015, **243**, 195-198.

8   A. Sanchez, S. Abbet, U. Heiz, W. D. Schneider, H. Häkkinen, R. N. Barnett and U. Landman, *J. Phys. Chem. A.*, 1999, **103**, 9573-9578.

9   E. Yoo, T. Okata, T. Akita, M. Kohyama, J. Nakamura and I. Honma, *Nano Lett.*, 2009, **9**, 2255-2259.

10 C. An, S. Peng and Y. Sun, *Adv. Mater.,* 2010, **22**, 2570-2574.

11 K. Soukup, P. Topka, V. Hejtmánek, D. Petráš, V. Valeš and O. Šolcová. *Catal. Today,* 2014, **236**, 3-11.

12 R. G. Chaudhuri and S. Paria, *Chem. Rev.*, 2012, **112**, 2373–2433.

13 J. M. Thomas, B. F. G. Johnson, R. Raja, G. Sankar and P. A. Midgley, *Acc. Chem. Res.*, 2003, **36**, 20-30.

14 M Liu, R Z Zhang, and W Chen, *Chem. Rev.*, 2014, **114**, 5117-5160.

15 Y. Zhou, H. Wang, M. Gong, Z. Sun, K. Cheng, X. Kong, Z. Guo and Q. Chen, *Dalton. trans.*, 2013, **42**, 9906-9913.

16 M B. Gawande, R. Zboril, V. Malgras and Y. Yamauchi, *J. Mater. Chem. A.*, 2015, **3**, 8241-8245.

17 M B. Gawande, P S. Branco and R S. Varma, *Chem. Soc. Rev.,* 2013, **42**, 3371-3393.

18 S. Sá, M B. Gawande, A. Velhinho, J. P. Veiga, N. Bundaleski, J. Trigueiro, A. Tolstogouzov, O. M. N. D. Teodoro, R. Zboril, R S. Varma and P S. Branco, *Green Chem*., 2014, **16**, 3494-3500.

19 M B. Gawande, R. Luque and R. Zboril, *ChemCatChem*, 2014, **6**, 3312-3313.

20 D. Wang. *Astruc. Chem. Rev.*, 2014, **114**, 6949-6985.

21 H. Hildebrand, K. Mackenzie and F D. Kopinke, *Environ. Sci. Technol.*, 2009, **43**, 3254–3259.

22 Z. Sun, J. Yang, J. Wang, W. Li, S. Kaliaguine, X. Hou, Y. Deng and D. Zhao, *J. Mater. Chem. A.*, 2014, **2**, 6071-6074.

23 Q M. Kainz and O. Reiser, *Acc. Chem. Res.*, 2014, **47**, 667-677.

24 X. Le, Z. Dong, Y. Liu, Z. Jin, T. Huy, M. Le and J. Ma, *J. Mater. Chem. A.*, 2014, **2**, 19696-19706.

25 X. X. Han, A. M. Schmidt, G. Marten, A. Fischer, I. M. Weidinger and P. Hildebrandt, *ACS Nano*, 2013, **7**, 3212-3220.

26 J. Cao, J. C. Li, L. Liu, A. J. Xie, S. K. Li, L. G. Qiu, Y. P. Yuan and Y. H. Shen *J. Mater. Chem. A.*, 2014, **2**, 7593-7597.

27 Z. J. Wu, C. G. Sun, Y. Chai and M. G. Zhang, *RSC Advances*, 2011, **1**, 1179–1182.

28 X. B. Zhang, H. W. Tong, S. M. Liu, G. P. Yong and Y. F. Guan, *J. Mater. Chem. A.*, 2013, **1**, 7488-7494.

29 Q M. Kainz, R. Linhardt, R N. Grass, G. Vilé, W J. Stark, O. Reiser, *Adv. Funct. Mater*. 2014, **24**, 2020–2027.

30 M B. Gawande, Y. Monga, R. Zboril, R K. Sharma, *Coordin. Chem. Rev*., 2015, **288**, 118-143.

31 R. Li, P. Zhang, Y. Huang, P. Zhang, H. Zhong and Q. Chen, *J. Mater. Chem. A.*,2012, **22**, 2275-22755.

32 T. Yao, T. Cui, J. Wu, Q. Chen, X. Yin, F. Cui and K. Sun, *Carbon*, 2012, **50**, 2287-2295.

33 T. Zeng, X. Zhang, S. Wang, Y. Ma, H. Niu and Y. Cai, *Chem - Eur. J.*, 2014, **20**, 6474-6481.

34 O. O. Fashedemi, H. A. Miller, A. Marchionni, F. Vizza and K. I. Ozoemena, *J. Mater. Chem. A.*,2015, **3**, 7145-7156.

35 M. Shokouhimehr, T. Kim, S. W. Jun, K. Shin, Y. Jang, B. H. Kim, J. Kim and T. Hyeon, *Appl. Catal. A: Gen.*, 2014, **476**, 133-139.

36 B. Liu, Q. Wang, S. Yu, T. Zhao, J. Han, P. Jing, W. Hu, L. Liu, J. Zhang, L. Sun and C. Yan, *Nanoscale*, 2013, **5**, 9747-9757.

37 B. Liu, Y. Niu, Y. Li, F. Yang, J. Guo, Q. Wang, P. Jing, J. Zhang and G. Yun, *Chem. Commun.,* 2014, **50**, 12356-12359.

38 Y. Deng, Y. Cai, Z. Sun, J. Liu, C. Liu, J. Wei, W. Li, C. Liu, Y. Wang and D. Zhao, *J. Am. Chem. Soc.,* 2010, **132**, 8466-8473.

39 X. Li, X. Wang, D. Liu, S. Song and H. Zhang, *Chem. Commun.,* 2014, **50**, 7198-7201.

40 G. Cheng, J. Zhang, Y. Liu, D. Sun and J. Ni, *Chem. Commun.,* 2011, **47**, 5732-5734.

41 S. Zhang, J. Li, W. Gao and Y. Qu, *Nanoscale*, 2015, **7**, 3016-3021.

42 T J. Yao, T Y. Cui, X. Fang, J. Wu, *Nanoscale*, 2013, **5**, 5896-5904.

43 F. Lin, D T. Hoang, C. K. Tsuang, W Y. Huang, P D. Yang, *Nano Res.* 2011, **4**, 61-71.

44 Q. Wang, W J. Jia, B C. Liu, X. Gong, C Y. Li, P. Jing, Y J. Li, G R. Xu, J. Zhang. *J. Mater. Chem. A*, 2013, **1**, 12732–12741.

45 J. Liu, Z K. Sun, Y H. Deng, Y. Zou, C Y. Li, X H. Guo, L Q. Xiong, Y. Gao, F Y. Li and D Y. Zhao, *Angew. Chem. Int. Ed*, 2009, **48**, 5875-5879.

46 M Y. Zhou and G W. Diao, *J. Phys. Chem. C.*, 2011, **115**, 24743-24749.

47 A. S. Diez, M. G. Mayer, M. A. Volpe, *Appl. Catal. A: Gen.*, 2014, **482**, 24-30. 43

48 V. Polshettiwar, R. Luque, A. Fihri, H B. Zhu, M. Bouhrara, J M. Basset, *Chem. Rev.*, 2011, **111**, 3036-3075.

49 J. Liu, S Z. Qiao, Q H. Hu, G Q. Lu, *Small*, 2011, **4**, 425-443.

50 Y H. Deng, Y. Cai, Z K. Sun, D Y. Zhao, *Chem. Phys. Lett.*, 2011, **510**, 1-13.

51 G. Chen, Y. Zhao, G. Fu, P. N. Duchesen, L. Gu, Y. Zheng, X. Weng, M. Chen, P. Zhang and C.W. Pao, N. F. Zhen, *Science*, 2014, **344**, 495-499.

52 J. Shi, *Chem. Rev.*, 2012, **113**, 2139-2181.

53 S. Tsunekawa, K. Ishikawa, Z.-Q. Li, Y. Kawazoe and A. Kasuya, *Phys. Rev. Lett.*, 2000, **85**, 3440-3443.

54 Y. Y. Chu, Z. B. Wang, Z. Z. Jiang, D. M. Gu and G. P. Yin, *Adv.Mater.*, 2011, **23**, 3100-3104.

55 Q. Wang, Y J. Li, B C. Liu, Q. Dong, G R. Xu, L. Zhang, *J. Mater. Chem. A*, 2015, **3**, 139-147.

56 M. F. Camellone and S. Fabris, *J. Am. Chem. Soc*., 2009, **131**,10473-10483.

57 H. Y. Kim, H. M. Lee and G. Henkelman, *J. Am. Chem. Soc*., 2012, **134**, 1560-1570.

58 Y. G. Wang, D. Mei, J. Li and R. Rousseau, *J. Phys. Chem. C*, 2013, **117**, 23082-23089.

59 Y. Wang, F. Wang, Q. Song, Q. Xin, S. Xu and J. Xu, *J. Am. Chem. Soc*., 2013, **135**, 1506-1515.

60 J. Shi, *Chem. Rev.*, 2012, **113**, 2139-2181.
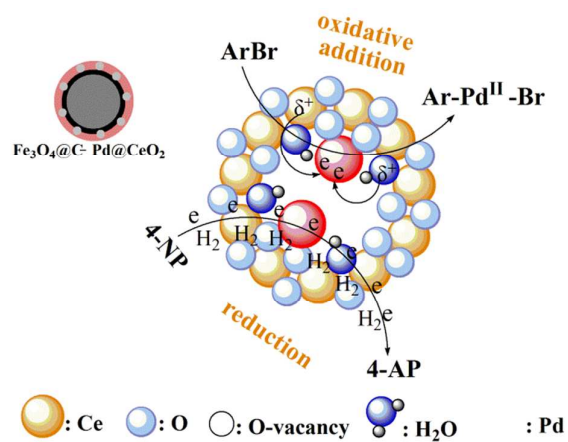
The novel multifunctional Fe_3O_4@C-Pd@CeO_2 nanospheres show excellent catalytic performance in the Suzuki–Miyaura cross-coupling reaction and the reduction of 4-nitrophenol